Stability and nonlinear evolution of electrolyte films on substrates with spatially periodic charge density

Mahnprit S. Jutley[1] and Vladimir S. Ajaev[1,2,*]
[1]*Department of Mathematics, Southern Methodist University, Dallas, Texas 75275, USA*
[2]*Kutateladze Institute of Thermophysics SB RAS, Novosibirsk 630090, Russia*

(Received 19 May 2018; revised manuscript received 31 July 2018; published 25 September 2018)

The stability of a thin electrolyte film on a substrate characterized by a spatially periodic electrical charge density is considered. Using the Debye-Hückel approximation to model the electrostatic potential and the lubrication-type framework for the viscous flow description, we derive a strongly nonlinear evolution equation for the film thickness. Linear stability analysis is carried out using a combination of numerical techniques for finding the eigenvalues of the discretized stability problem, asymptotic methods valid for small charge density variation, and Floquet theory. Substrate charge nonuniformity can have either stabilizing or destabilizing effect. For the important practical case of a liquid film with boundary charge densities of opposite signs and thickness comparable to the Debye length, transition from stabilizing to destabilizing influence is observed as the patterning wavelength is decreased. A simple analytical estimate of the condition for such transition is provided. Weakly nonlinear regime is studied using analytical techniques. Numerical simulations of the strongly nonlinear evolution of the film are conducted, with emphasis on competition between patterns induced by substrate charge nonuniformity and by the intrinsic nonlinearity present even for uniformly charged substrate.

DOI: 10.1103/PhysRevE.98.032803

I. INTRODUCTION

The rupture of thin liquid films on solid surfaces is important to numerous current and emerging engineering applications. In microfluidics, the efficient transport of drops, bubbles, or biological cells through microchannels is essential for proper operation of many microscale devices [1,2]. In order for high transport rates to be achieved and maintained, the drop, bubble, or cell must remain separated from the wall by a liquid film; this cannot be achieved if there is an occurrence of film rupture. For cooling of electronic devices [3,4] and thermal management systems for outer space applications [5,6] avoiding film rupture is essential for the prevention of extreme change of heat flux due to the appearence of dry patches on hot surfaces.

Viscous flows in thin liquid layers have been investigated by numerous authors and in various frameworks following the foundational work of Reynolds [7] on the theory of lubrication. Thorough reviews by Oron *et al.* [8] and Craster and Matar [9] discuss thin liquid films that have been exposed to various mechanical, thermal, or structural factors. Under such circumstances, phenomena such as thermocapillary spreading, fingering instabilities, and dry spot formation can occur. The conditions of rupture are considered to be well understood for a film bounded by a deformable fluid interface and a *homogenous flat* solid substrate. Ruckenstein and Jain [10] established the linear stability criteria for such films under the action of London–van der Waals dispersion forces. Williams and Davis [11] and Burelbach *et al.* [12] considered the nonlinear evolution of such thin liquid films and found that system nonlinearities speed up the development of the instability driven by London–van der Waals forces. Similarity solutions near the point of rupture under the action of London–van der Waals forces were found by Zhang and Lister [13], who also conducted simulations of the nonlinear evolution of the film thickness showing that instability leads to film rupture in a finite amount of time.

While previous studies focused on film rupture driven by London–van der Waals forces, another mechanism to consider is rupture due to electrostatic effects. These effects, which have been encountered experimentally [14], show readily since many liquids contain ions and electrical double layers can form near charged interfaces as shown in Graciaa *et al.* [15] and Li and Somasundaran [16]. In a recent study, Ketelaar and Ajaev [17] consider the stability of a thin electrolyte film on a uniformly charged solid substrate within the framework of the Debye-Hückel approximation for electrostatic potential. The effects of charge regulation parameters at interfaces and electrolyte properties are used to formulate stability criteria. It is shown that there is a critical film thickness related to the Debye screening length at which the film ruptures and this critical film thickness depends on the charge regulation conditions at the interfaces.

The stability of liquid films on *patterned or structured* solid surfaces has been an active area of research for several decades [18]. A patterned surface is a flat surface with periodic variation in chemical properties, such as alternating squares or stripes. A structured surface is characterized by periodic variations in topography, such as periodic arrays of parallel grooves or arrays of pillars. Unstable films on chemically patterned surfaces were studied extensively [19–23] in the context of fabrication processes based on dewetting of heterogeneous surface, e.g., when polymer films break up and

*ajaev@smu.edu

 ©2018 American Physical Society

form a regular pattern on a silicon surface with an array of metal stripes [24]. The regularity of the pattern obtained by this method depends on the relative magnitude of the instrinsic wavelength of the instability and the scale of the substrate heterogeneity.

Structured surfaces have been discussed in the context of drag reduction in various microfluidic devices [25], with the main focus on the so-called Cassie-Baxter state corresponding to the case when gas is trapped inside the structure, e.g., in the grooves or in spaces between the pillars. As with nonstructured walls, efficient transport of drops and bubbles in channels with structured walls is only possible if they remain separated from the walls by a liquid film. Stability of such film was investigated by Ajaev *et al.* [26] under conditions when the cause of film rupture is the action of London–van der Waals disjoining pressure. The stabilizing role of surface tension leads to a characteristic instability wavelength which can differ significantly from the wavelength of the structure.

While there is a significant amount of work on film break-up on patterned and structured surfaces, the situation when film break-up is driven by electrostatic forces and the substrate charge is nonhomogeneous received very little attention, despite its importance for applications. For example, in biological systems, the boundary condition of uniform charge density is almost never realized [27]. The objective of the present study is to investigate the effect of boundary charge nonuniformity in the context of a simple configuration of a liquid layer on a charged substrate. We note that the main challenges here stem from the fact that the base state for the corresponding stability problem is not homogeneous. In the present study, we address this challenge though a combination of numerical and analytical approaches, resulting in comprehensive analysis of the stability conditions.

We consider a model with fixed spatially periodic substrate charge density. Both types of substrates discussed above, patterned and structured, are relevant under the scope of spatially periodic charge density. Since materials with different chemical properties often have inherently different charge densities, a patterned surface can be represented by a substrate with spatially periodic charge density. Also, our study leads to a way of representing a structured surface in the Cassie-Baxter state, and that is to consider a thin electrolyte film in which the charge density of the menisci of the gas-filled grooves differs from that of the solid surface. While we expect our approach to have a wide range of applications, it is also important to recognize its limitations. They mostly stem from the fact that we focus on the instabilities which are driven by electrostatic effects and consider other factors, such as surface roughness and chemical heterogeneity not related to charge variation, to be secondary. These factors are neglected in our formulation.

The paper is organized as follows. In Sec. II, the model is presented and formulated nondimensionally and an evolution equation for film thickness is discussed, valid when the liquid layer thickness is much smaller than the relevant horizontal length scales. Section III begins with a review of the linear stability results for the special case of spatially uniform substrate charge density. The case of spatially periodic substrate charge density is then tackled in Secs. III and IV using a combination of asymptotic expansions, Floquet theory, weakly nonlinear analysis, and numerical simulations. Discussion of the results and conclusions are contained in Sec. V.

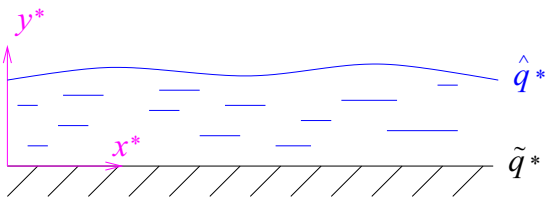

FIG. 1. Sketch of the electrolyte film on substrate with periodic spatial variation of charge density.

II. FORMULATION

A thin film of liquid with viscosity μ and surface tension σ is on a solid substrate that is characterized by a periodic spatial variation of the charge density, $\tilde{q}^*$, with the average value equal to q_a^*. The system is modeled in Cartesian coordinates x^* and y^*, where (*) will denote all dimensional variables. The geometric configuration is illustrated in Fig. 1. The liquid is an electrolyte with N different types of ions of valencies z_k and bulk concentrations $n_k^{(0)}$ $(k = 1, 2, \ldots, N)$. Near electrically charged interfaces, formation of electrical double layers can be expected. Their characteristic width is defined by the Debye length λ_D,

$$\lambda_D = \sqrt{\frac{\epsilon k_B T}{e^2 \sum_{k=1}^{N} n_k^{(0)} z_k^2}}, \tag{1}$$

where ϵ is the electric permittivity of the liquid, k_B is the Boltzmann constant, and T is the temperature. The electrostatic potential, ψ^*, is found using the Debye-Hückel approximation formulated together with the Stokes flow equations for incompressible liquid. The electrostatic effects related to the presence of the substrate charge and the liquid surface charge ($\hat{q}^*$) can cause film instabilities. The case is considered where the disjoining pressure is dominated by the electrostatic effects with the London–van der Waals contribution being negligible for the range of film thickness values considered here. The nondimensional charge densities and electrostatic potential are defined as

$$\hat{q} = \frac{\hat{q}^*}{q_a^*}, \quad \tilde{q} = \frac{\tilde{q}^*}{q_a^*}, \quad \psi = \frac{\epsilon \lambda_D^{-1} \psi^*}{q_a^*}. \tag{2}$$

The base state of the film has an average thickness d. The characteristic velocity U of the viscous flow induced by the instability is found from the balance among electrostatic, capillary, and viscous contributions to stresses during film deformation,

$$U = \frac{q_a^{*3}}{\mu \sigma^{1/2}} \left(\frac{d}{\epsilon} \right)^{3/2}. \tag{3}$$

The capillary number for this flow, $\mathrm{Ca} = \mu U/\sigma$, is typically small, which, together with the assumption of small aspect ratio for the liquid layer, allows us to apply the standard tools of the lubrication-type analysis. The corresponding derivation, described in Appendix A, leads to a nondimensional evolution

equation for film thickness $h(x,t)$ of the form

$$h_t + [h^3(h_{xxx} - \hat{q}\hat{q}_x)]_x = 0. \tag{4}$$

The scaled liquid surface charge density $\hat{q}$ can now be expressed in terms of h using the Debye-Hückel approximation to the Poisson-Boltzmann equation. Using the scales and assumptions formulated in Appendix A, the equation for the electric potential in the film is

$$\psi_{yy} = \kappa^2\psi, \qquad \kappa = \frac{d}{\lambda_D}. \tag{5}$$

At the liquid-air interface, the electrostatic potential will be considered to be fixed such that $\psi(x,h) = \hat{\psi}$. Thus, we consider a situation when charge transport and regulation results in redistribution of charges, so that $\hat{q}$ is nonuniform. At the liquid-substrate interface, the effect of substrate charge on the electrical field in the film is represented by

$$\psi_y(x,0) = -\kappa\tilde{q}, \tag{6}$$

where $\tilde{q}$ is the spatially periodic substrate charge density. Note that the contribution from the electrical field in the substrate is neglected here. While solving the equations for the electric field in the substrate could be added in the formulation, as is done in some studies [28], the assumption of small thickness of the liquid film together with high relative dielectric permittivity of liquids such as water compared to that of typical dielectric substrates allow one to justify our approach.

Using condition (6) and the fixed free surface potential condition for the electrostatic potential governed by Eq. (5), the expressions for the electrostatic potential distribution in the film and the free surface charge density are

$$\psi = [\hat{\psi} + \tilde{q}(x)(\cosh\kappa h + \sinh\kappa h)]\frac{\cosh\kappa y}{\cosh\kappa h} - \tilde{q}(x)(\cosh\kappa y + \sinh\kappa y), \tag{7}$$

$$\hat{q}(x,h) = [\hat{\psi}\sinh\kappa h - \tilde{q}(x)]\,\mathrm{sech}\,\kappa h. \tag{8}$$

Thus, $\hat{q}$ appearing in Eq. (4) is now expressed in terms of the function $h(x,t)$ and the specified substrate charge density $\tilde{q}(x)$. In most of our derivations and simulations we use

$$\tilde{q}(x) = 1 + \delta\cos(\pi x/L), \tag{9}$$

although we also verified that using a superposion of several sinusoidal functions instead of the second term on the right-hand side of Eq. (9) does not alter any of the key conclusions presented below. Two new nondimensional parameters enter the formulation through Eq. (9), the amplitude δ and the length scale L of the spatial variation of the substrate charge density. Together with the ratio κ of the film thickness to the Debye length, these represent the key parameters we vary in our scaled model.

III. LINEAR STABILITY

A. Linear stability of uniform film

Let us briefly review the classical linear stability analysis results for the limiting case when the substrate charge density is uniform ($\delta = 0$). Although Eq. (4) is nonlinear, it has a simple steady-state solution that corresponds to a uniform film thickness, $h(x,t) = 1$. The behavior of a small perturbation $\zeta(x,t)$ to this solution is described by the linearization of Eq. (4),

$$\zeta_t + \zeta_{xxxx} - G\zeta_{xx} = 0, \qquad G \equiv [\hat{q}\hat{q}_h]_{h=1}. \tag{10}$$

Based on Eq. (10), the growth rate γ of a small sinusoidal perturbation with wave number k is determined to be

$$\gamma(k) = -k^2(G + k^2). \tag{11}$$

A perturbation of an arbitrary wave number will always decay for a non-negative G, indicating stability. The film becomes unstable when the condition $G < 0$ is satisfied.

By substituting the expression for G based on $\tilde{q}(x)$ from (9) with $\delta = 0$ into Eq. (11), a quadratic equation with respect to $\hat{\psi}$ is formed of which its two roots

$$\hat{\psi} = -\sinh\kappa, \quad \frac{1}{\sinh\kappa}, \tag{12}$$

are the stability branches for the $\hat{\psi}$-κ plane. These are shown in Fig. 2.

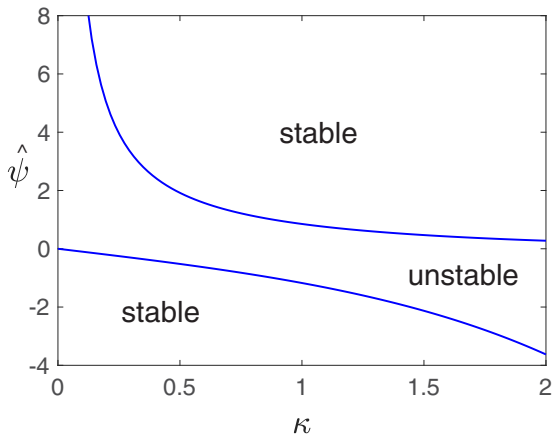

FIG. 2. Stability diagram for the liquid film on a uniformly charged solid substrate.

In order to interpret this stability diagram, it is useful to recall that according to (8) the scaled liquid surface charge density in the limit of uniform substrate charge is

$$\hat{q} = (\hat{\psi}\sinh\kappa - 1)\,\mathrm{sech}\,\kappa, \tag{13}$$

where according to (2) $\hat{q}$ can be interpreted as the ratio of dimensional charge densities for the two interfaces. We note that it is not immediately obvious that having oppositely charged surfaces should lead to instability and vice versa since such simplified view does not account for interactions of surface charges with ions in the screening layers in the liquid near charged interfaces. The analysis leading to the stability curves shown in Fig. 2 accounts for all these interactions. The stability region seen above the upper curve ($\hat{\psi}\sinh\kappa > 1$) corresponds to $\hat{q} > 0$, as readily seen from the above expression for $\hat{q}$. This is consistent with the rule of repulsion of charged surfaces of the same sign across electrolyte, established in the classical studies of Langmuir [29] and Parsegian and Gingell [30] and since confirmed by numerous experimental and theoretical studies. The justification for this rule is based on the following argument from the classical theory of electrical

double layers [31]. Consider a flat uniformly charged interface. Then, a cloud of screening charge of the opposite sign will be formed in the liquid near the interface resulting in gradients of ion concentration and thus creating osmotic pressure gradient. It is this osmotic pressure gradient that compensates for the electrostatic attraction between the interfacial charges and the screening charges. As two double layers start overlapping, the high osmotic pressure in the liquid layer between the interfaces is the key factor that ensures repulsion between them and thus leads to a stable liquid film.

For the oppositely charged surfaces, i.e., under the top curve, Fig. 2 shows instability for a range of conditions. For example, if $\hat{\psi} = 0$, the system is always unstable. This can be explained by the method of images. All charges, including the ones on interface and the ions in the solution, interact with their electrostatic images with respect to the liquid-gas interface. Since that interface is at a constant potential of $\hat{\psi} = 0$, the images are of the opposite charge and thus the interaction is attractive, leading to destabilization. However, the condition of $\hat{q} < 0$ does not always guarantee instability. Clearly, there is a region of stability under the bottom curve in Fig. 2. This stabilization occurs when sufficient concentration of ions is reached in the liquid layer so that the total interfacial charge is neutralized. This effect becomes stronger as the layer thickness is decreased, i.e., below a certain critical value of κ, as indeed is seen in Fig. 2 (lower curve).

Let us now discuss the question of film stability when the substrate charge density is nonuniform. The naive approach to solving this problem would be to use the average value of the substrate charge density and look up the corresponding point on the stability diagram of Fig. 2. Our analysis will identify situations when such approach is reasonable (stability threshold does not change significantly as a result of spatial nonuniformity) versus situations where it fails to accurately predict the threshold. In other words, we consider the question of how sensitive the system is to nonuniformity of the substrate charge under different conditions.

Our objective in the rest of this Section will be to determine how the stability diagrams will change as a result of spatial variation of the substrate charge density. We note that under these conditions, the steady state is no longer that of uniform thickness. Let us first discuss the steady states and then study their stability.

B. Nonuniform base state

The solution corresponding to liquid film of uniform thickness ($h(x,t) = 1$), used as the base state in the classical stability analysis above, is not consistent with the spatially periodic variation of the substrate charge density. However, steady-state solutions still exist in that case and can be obtained by setting all temporal derivatives in our formulation to zero. Finding such solutions is the main objective of the present subsection. Whether or not such solutions can be observed experimentally depends on their stability, which is the subject of the analysis in the subsections to follow.

Steady-state solutions of Eq. (4) with $\hat{q}(x,h)$ and $\tilde{q}(x)$ given by (8) and (9), respectively, have been found by first discretizing the spatial derivatives on the domain $[-L, L]$ and then solving the resulting system of first-order differential

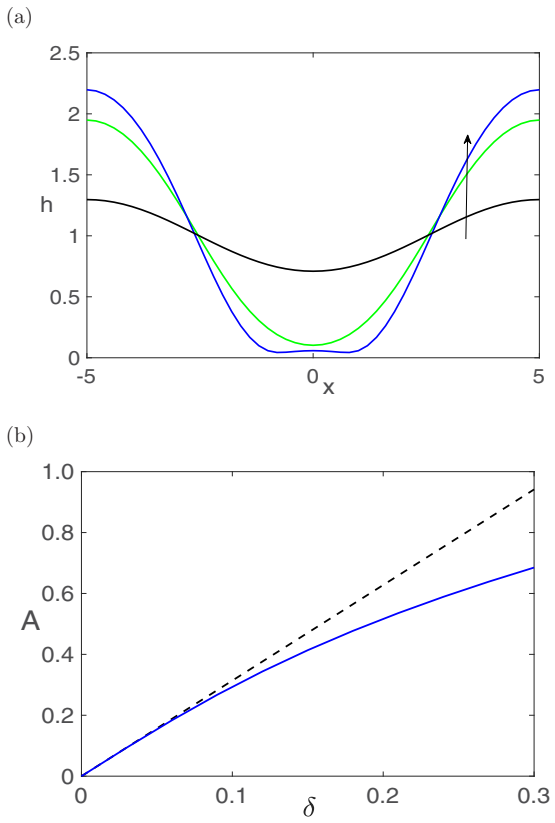

FIG. 3. (a) Steady interface shapes for $L = 5$, $\kappa = 1$, $\hat{\psi} = -1$, and the values of δ increasing in the direction of the arrow: $\delta = 0.1$ (black line), $\delta = 0.5$ (green), and $\delta = 1$ (blue). (b) Amplitude of the interface deformation as a function of δ obtained from the numerical solution (solid line) and from the linearized equation (dashed line).

equations in MATLAB using the `ode15s` subroutine until the change in the solution norm falls below the specified tolerance. Figure 3(a) shows steady interface shapes for three different values of δ. Note that at larger δ, simple sinusoidal variation of substrate charge density does not translate into an equally simple shape of the interface. This is clearly a sign of the intrinsic nonlinearity of the system.

For small values of δ, an approximate expression for the base state can be derived. Since the steady-state solution implies constant pressure in the liquid, Eq. (A7) from Appendix A can be used to formulate a simplified equation for the steady state,

$$h_{0xx} - \frac{1}{2}\hat{q}^2 = C. \tag{14}$$

By substituting an asymptotic expansion

$$h_0 = 1 + \delta h_0^{(1)} + \delta^2 h_0^{(2)} + \ldots \tag{15}$$

into Eq. (14) and neglecting the $O(\delta^2)$ contributions, we obtain

$$h_0^{(1)} = A\cos(\pi x/L), \quad A = \frac{\hat{\psi}\sinh\kappa - 1}{\cosh^2\kappa}\left(\frac{\pi^2}{L^2} + G\right)^{-1}, \tag{16}$$

where the same definition of the nondimensional parameter G is used as above in Eq. (10). The result can be compared

with the numerical solution, providing a useful validation test. The comparison of solution amplitudes is given in Fig. 3(b). Clearly, the asymptotic method gives accurate approximation of the interface deformation up to $\delta \approx 0.1$.

Once the steady-state solution is found on the domain of length $2L$, periodic extension can be used to define the base state, $h_0(x)$, on the entire computational domain. Let us now turn to the important issue of the stability of this solution.

C. Linear stability: Discrete eigenvalue problem approach

A small time-dependent perturbation $\zeta(x,t)$ of the base state $h_0(x)$ satisfies the linearized version of the Eq. (4), which can be conveniently written in the form

$$\zeta_t + h_0^3\zeta_{xxxx} + 3h_0^2 h_{0x}\zeta_{xxx} - h_0^3 Q\zeta_{xx} - \left[2h_0^3 Q_x + 3h_0^2 h_{0x} Q\right]\zeta_x - 3h_0^2 h_{0x} Q_x \zeta = 0, \tag{17}$$

where we define $Q \equiv \hat{q}(h_0)\hat{q}_h(h_0)$. The numerical method for solving Eq. (17) is described in Appendix B. The resulting stability curves will be plotted in the same coordinates as in Fig. 2 to facilitate easier comparison with the case of uniform charge density. In the discussion below, our focus is on the modification of the *lower* stability curve of Fig. 2 for the following two reasons: (i) reported experimental observations of film rupture by electrostatic forces typically involve interfacial charges of opposite sign, which in our formulation corresponds to negative $\hat{\psi}$, and (ii) the modification of the upper stability curve by the charge patterning tends to be much smaller than that of the lower stability curve.

The choice of the parameter L, the nondimensional length scale of the substrate charge density variation, requires special discussion. It has been shown in the previous studies that when the instability wave number is equal to the substrate patterning wave number or one of its integer multiples, dramatic changes in the instability growth rate can occur, a phenomenon known as resonance. This phenomenon has been well studied [23,32]. However, due to the long-wave nature of the instability considered here, the most unstable modes are likely to have a wavelength which is orders of magnitude larger than the scale of the patterning, the latter typically corresponding to micro- and nanoscale. In this regime, which is the focus of the present study, the effect of resonant interaction is negligible but, as we shall see, the effect of substrate charge patterning is not. To explore this regime, let us start with $L_T = 50$ and $L = 5$ and then gradually reduce L to account for finer scales of charge patterning.

Figure 4 illustrates the changes in the lower stability branch of Fig. 2 as a result of patterning. According to Fig. 2, when the scaled potential $\hat{\psi}$ is decreased for a fixed κ, transition to the stable regime takes place at a certain critical value of the potential denoted by $\hat{\psi}_c$ here and below. The *magnitude* of this quantity is shown in both parts of Fig. 4 by the dashed blue lines. When substrate charge nonuniformity is introduced according to Eq. (9) with $\delta = 0.05$ and $L = 5$, the new magnitude of the critical potential corresponds to the black solid line in Fig. 4(a). Let us discuss the result shown in the figure. First, in the limit of $\kappa \to 0$ the Debye length is much larger than the film thickness and the electric field in the film becomes nearly uniform. This implies essentially

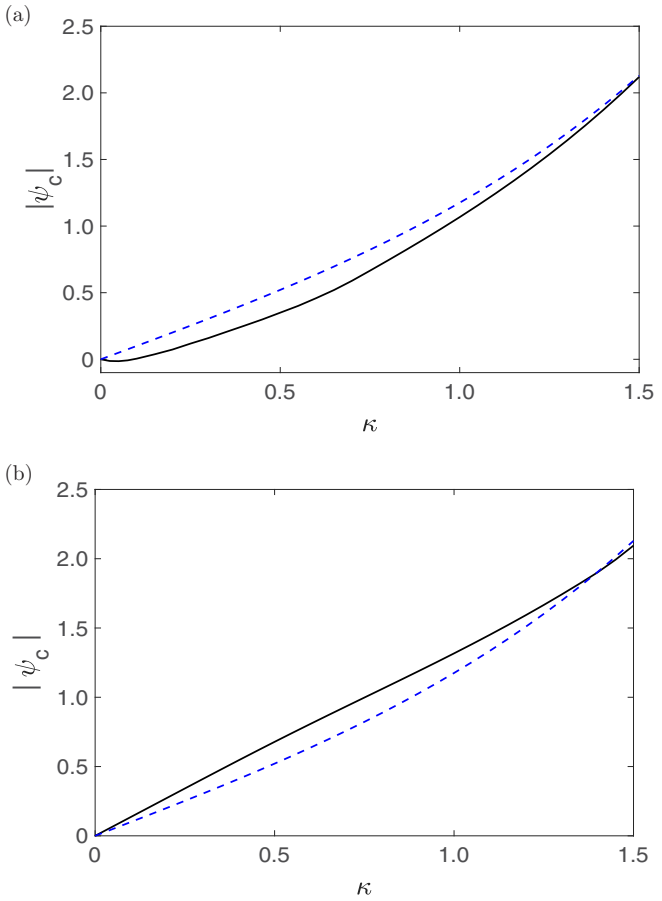

FIG. 4. The magnitude of the negative scaled potential at the transition between the stable and unstable films plotted for $\delta = 0.05$ (black solid lines) and two values of the nondimensional charge patterning length: (a) $L = 5$, (b) $L = 2.5$. The uniformly charged substrate results are shown by blue dashed lines for comparison.

no double layer structure, and the neutral stability condition should be $\hat{\psi} = 0$. This is indeed seen in the figure. However, as κ is increased, the correction to the stability criterion quickly comes into play and the effect of charge patterning is found to be stabilizing for a range of κ. In relative terms, stabilization tends to be more significant at smaller values of κ. For example, at $\kappa = 0.5$, the critical value changes from 0.521 to 0.350, a significant drop given the relatively small value of δ. The effect becomes weaker as κ is increased and eventually slightly destabilizing influence is observed at κ near 1.5 and above. This destabilization, however, may be difficult to see experimentally since it requires the fluid interface charge density to be significantly larger than that of the solid substrate, which is an unlikely scenario.

To investigate the effect of the length scale of the charge patterning, we reduced the value of L for fixed δ and found that the correction to the stability criterion decreases with L. Furthermore, for a given κ, the effect changes sign at some critical value of L. As the value of L is decreased further, the interface becomes destabilized by the patterning over a range of κ previously showing stabilization. This result is illustrated for $L = 2.5$ in Fig. 4(b). Note that reducing the pattern length by a factor of two while keeping all other parameters the

same resulted in the dramatic qualitative change in how the patterning affects film stability: from mostly stabilizing in Fig. 4(a) to mostly destabilizing in Fig. 4(b). It is intuitive to expect that higher amplitude of charge nonuniformity can potentially lead to a more significant shift in the stability conditions. However, the scale of charge variation is often considered a secondary factor unless such variation happens to produce a resonant interaction between the substrate pattern and the perturbation of the free surface of the liquid layer [23]. Our simulations indicate that even in the nonresonant case, the effect of change of the wavelength of substrate charge variation can be significant. This shows that for practical applications, not only the amplitude but also the spatial scale of substrate charge variation has to be specified to determine the liquid layer stability conditions on such substrates.

D. Linear stability for small δ

For the case of small δ and nonresonant interaction, the shift in the instability threshold due to substrate charge patterning can be found analytically using asymptotic methods. Before presenting the results of such analysis, let us discuss the general expectations of the behavior at small δ. It may seem that in the absence of resonance, the correction to stability criterion should stem from a shift in the average values of the coefficients in the linearized problem, implying that at small δ it is of the order of δ^2. However, using such an estimate at $\kappa = 0.5$ results suggests a correction $\sim 10^{-3}$ rather than the actually observed shift of about 0.171. The apparent paradox is explained by the fact that the argument leading to δ^2 estimate is flawed: It actually does not account for the possibility of significant change in the characteristic wave number of the most unstable perturbation. In order to illustrate how such a change can happen, consider a model problem in which Eq. (10) is modified by an addition of the term $\delta^2\zeta$ on the left-hand side, resulting in the disperion relation

$$\gamma(k) = -k^2(G + k^2) - \delta^2. \tag{18}$$

It may appear that the extra term leads to an $O(\delta^2)$ change in the stability criterion compared to the case of $\delta = 0$, but in reality the change is $O(\delta)$, as becomes clear from the sketch in Fig. 5(a). First, the blue dashed line in the sketch corresponds to the dispersion curve at G above but very close to $G = 0$, which would be enough to induce the instability at $\delta = 0$. However, for the modified problem, Eq. (18), all points on the dashed dispersion curve are well below the instability threshold. It is only when G is increased to the point where the corresponding dispersion curve, the black solid line, touches the horizonal axis, that the instability can be observed at the critical wave number $k_c^2 \sim \delta$, indicating that G should also be of the same order. Thus, the shift in the stability threshold G compared to the original value of $G = 0$ is in fact a linear function of δ.

While the model problem corresponding to (18) is much simpler than the actual linear stability problem defined by (17), the stability corrections have essentially the same behavior. To verify this, we conducted detailed perturbation analysis for the full problem and found that for a range of realistic values of κ, the shift in stability criteria mostly originates from the last term of (17), i.e., the term $-3h_0^2 h_{0x} Q_x \zeta$. Based on

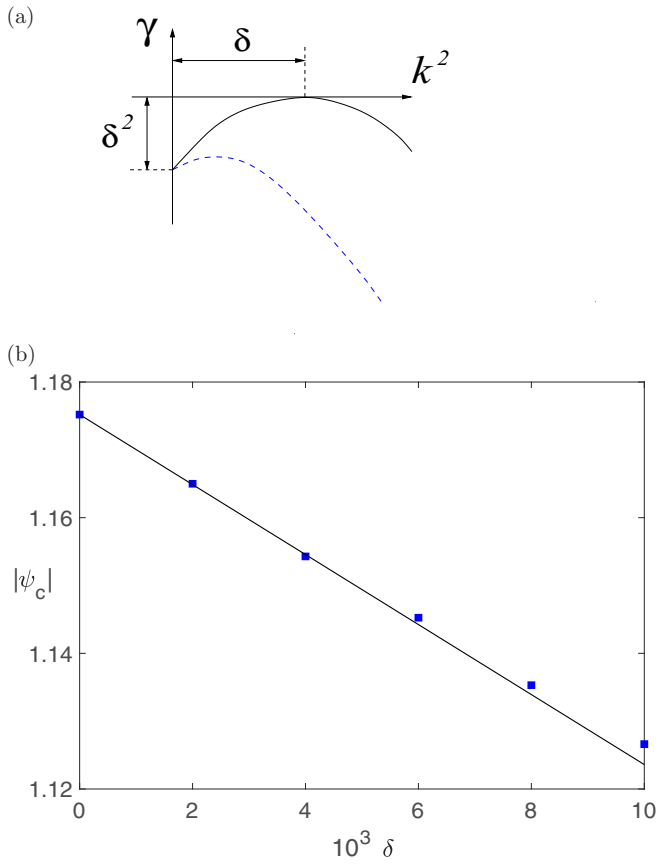

FIG. 5. (a) A sketch illustrating dispersion curve shapes for the model problem, Eq. (18), at values of G very close to zero (dashed blue line) and the value of G at the actual instability threshold (black solid line). (b) Comparison of the analytical stability criterion with the numerical one at $\kappa = 1$.

the nonuniform base state solution given by (16), we find the following leading-order approximations:

$$h_{0x} = -\delta\beta A \sin(\beta x) + O(\delta^2), \quad \beta = \frac{\pi}{L}, \tag{19}$$

$$Q_x = \delta\kappa\beta(\tanh\kappa + \kappa A)\sin(\beta x) + O(\delta^2). \tag{20}$$

Substituting these leading-order expressions into Eq. (17), we obtain results qualitatively similar to the ones illustrated by the simplified model of Eq. (18). In particular, the modified critical value of the scaled potential $\hat{\psi}$ is approximated by

$$\psi_c = -\sinh\kappa + \delta\kappa^{-1}\cosh\kappa\sqrt{6\kappa(\kappa\beta^{-2} - \tanh\kappa)}, \tag{21}$$

which is indeed a *linear* function of δ. This result corresponds to the black solid line in Fig. 5(b). Numerical results found by the method from the previous subsection, shown by the blue squares, are clearly in excellent agreement with the approximate model. This provides a useful verification of the numerical method we use.

Let us now use asymptotic method to explain the destabilizing effect seen in Fig. 4(b). The key to understanding this effect is that the average value of the leading-order term in the formula for Q_x changes sign at a critical value of the pattern

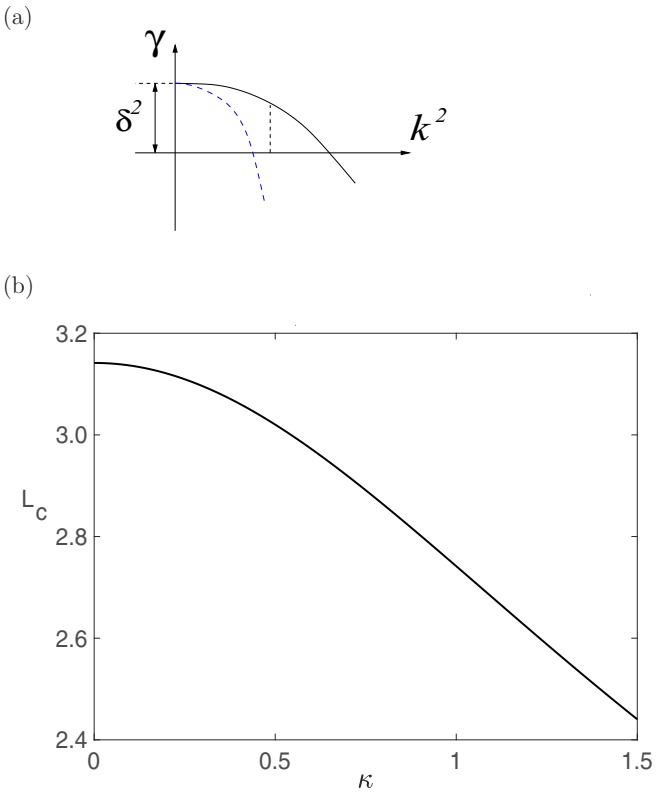

FIG. 6. (a) A sketch illustrating dispersion curves for positive average Q_x. (b) The plot of critical L for transition between stabilization and destabilization as a function of κ.

length scale,

$$L_c = \pi \left(\frac{\tanh \kappa}{\kappa} \right)^{1/2}. \tag{22}$$

With positive average Q_x, the qualitative change in the dispersion curve with δ is no longer described by the sketch shown in Fig. 5(a). In fact, the change of sign implies a shift in dispersion curves upward rather than downward, as shown schematically in Fig. 6(a). While in principle such shift could mean destabilization at any value of δ, in reality the stability condition is dictated by the size of the domain, L_T. If the minimum wave number that fits into the domain corresponds to the vertical dashed line in Fig. 6(a), the dashed curve corresponds to stability, while the solid line means instability. This explains the destabilizing effect seen in Fig. 4(b). The critical value L_c is shown as a function of κ in Fig. 6(b). We note that the qualitative changes in the dispersion curves illustrated by the sketches in Fig. 5(a) and 6(a) have not been captured by the previously published simplified models of films stability on charged substrates.

E. Floquet theory

In typical applications, the scale of the pattern can be many orders of magnitude smaller than the scale of the domain, making the approach from Sec. III B impractical and very difficult to extend to three-dimensional situations. The perturbation method from the previous subsection is limited by the condition of small values of δ. However, there is an alternative

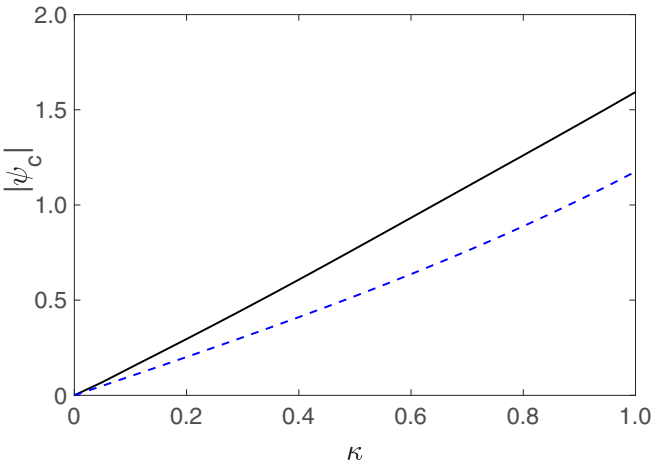

FIG. 7. Stability curve obtained using Floquet theory approach for $L = 2$, $\delta = 0.05$, with the dashed line showing the result for uniform charge density.

approach which requires numerical computation only on the interval of length L, i.e., the scale of the patterning, rather than on the scale of the instability. This method is based on the classical Floquet theory (also often called Floquet-Bloch theory) [23] and involves using the well-known theoretical result about the form of the solution of Eq. (17) as a superposition of terms $\sim e^{\gamma t + ikx}\hat{\zeta}(x)$, where $\hat{\zeta}$ is a periodic function on the interval of periodicity of the patterning. Based on (17), the equation for $\hat{\zeta}$ is

$$h_0^3 D_k^4 \hat{\zeta} + 3h_0^2 h_{0x} D_k^3 \hat{\zeta} - h_0^3 Q D_k^2 \hat{\zeta} - \left[2h_0^3 Q_x + 3h_0^2 h_{0x} Q\right] D_k \hat{\zeta} + \left(\gamma - 3h_0^2 h_{0x} Q_x\right)\hat{\zeta} = 0, \tag{23}$$

where $D_k = \frac{\partial}{\partial x} + ik$. The equation is then solved numerically using spectral discretization and with the minimum value of k chosen to simulate the finite-size domain used in the previous simulations ($L_T = 50$). Typical results for neutral stability found from this approach are shown in Fig. 7. The figure illustrates that the trend toward destabilization seen at larger L continues as the value of the scaled length is reduced further into the range where the discrete eigenvalue solution method becomes inefficient.

IV. NONLINEAR EVOLUTION

A. Limit of the uniformly charged substrate

In the limit of uniformly charged solid substrate, the evolution equation reduces to the classical problem of the form

$$h_t = [h^3(\varphi(h) - h_{xx})_x]_x, \tag{24}$$

where for our particular case $\varphi(h) = \hat{q}^2/2$. Weakly nonlinear analysis for the general equation (24) was carried out by several authors [23,33,34] in an effort to investigate the possibility of nonlinear stabilization of the instability of initially uniform base state $h \equiv 1$. To the best of our knowledge, this approach has not been applied to the models of stability of electrolyte films, so we carried out this calculation as described in Appendix C. The conclusion from the calculation

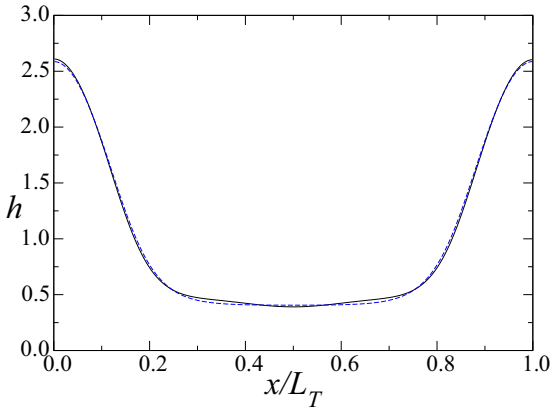

FIG. 8. Steady-state strongly nonlinear interface shapes at $\delta = 0.02$ (black solid line) with the result for the uniformly charged substrate ($\delta = 0$) shown for comparison by the dashed blue line.

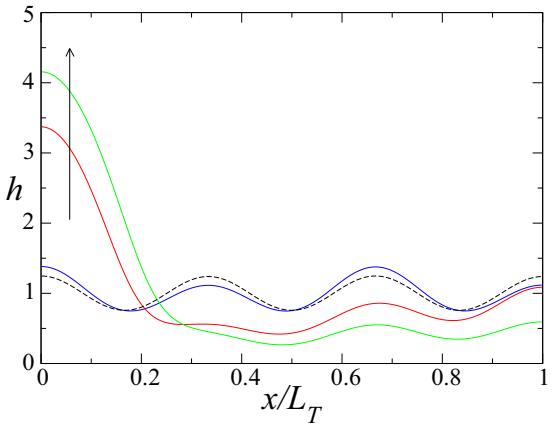

FIG. 9. Snapshots of interface shapes at different times showing the transition from the original pattern on the scale of substrate charge variation (black dashed line) to a strongly nonlinear solution of much larger amplitude; the arrow shows the order of snapshots in time, all results are for $\delta = 0.1$.

shown there is that *no* finite-amplitude nonlinear solutions are expected near the instability threshold.

The results of the weakly nonlinear analysis suggest that nonlinear stabilization does not occur near the bifurcation point but do not exclude the possibility of such stabilization in the strongly nonlinear regime. For many nonlinear equations, the only approach to investigating such possibility would be through extensive numerical simulations. However, for the model discussed here, additional insights into the behavior can be obtained by observing that if there is a finite amplitude solution in the strongly nonlinear regime, it has to satisfy the constant pressure condition along the interface, e.g.,

$$h_{xx} + \varphi(h) = C, \tag{25}$$

which is mathematically identical to the classical particle motion in a given potential (with x playing the role of the time variable). The situations is qualitatively similar to the case of thin films dewetting under the action of unbalanced intermolecular interactions described by disjoining pressure [35,36]. Using the analogy, we can expect strongly nonlinear steady-state shapes in our situation; these are indeed observed, as discussed in the next subsection.

B. Strongly nonlinear patterns

Let us now discuss the strongly nonlinear evolution and how it is affected by the spatial variation of substrate charge. We note that adding the nonuniformity introduces a new length scale (and thus potentially a new length scales of the pattern) which is independent from the length scale of the patterns discussed in the previous subsection. We conducted extensive numerical simulations to investigate how the strongly nonlinear evolution is modified by the effect of substrate patterning. Simulations are carried out for the original fully nonlinear equation, (4), using the numerical method described in the end of Appendix B. Let us first consider the effect of the amplitude of the charge variation, δ, on the strongly nonlinear dynamics.

For the case of uniform charge density, $\delta = 0$, we find steady-state strongly nonlinear solutions which are basically droplets connected by nearly flat thin film regions, as illustrated by the blue dashed line in Fig. 8. This is consistent with numerous observations reported in the framework of similar models in the limit of uniform substrate properties [23,36]. Let us now turn to how this solution changes as a result of underlying substrate patterning by gradually increasing the value of δ. Our first observation is that for small δ only minor modifications to the steady film shape are introduced, as can be seen from comparing the steady-state solution for $\delta = 0.02$ (solid line) with the case of uniform charge density in Fig. 8. However, as δ is increased, different dynamics is observed, which can be characterized by two stages. At the first stage, the solution rapidly approaches to the shape which has the same spatial periodicity as the substrate charge density, shown by a dashed line in Fig. 9 (for $\delta = 0.1$). However, there is also another stage, at which the interface spontaneously goes through another set of deformations and eventually approaches a new shape which is qualitatively similar to the ones in Fig. 8 except that the thin-film regions connecting the droplets show stronger deformation.

As the value of δ is increased further, the time for the transformation of the type shown in Fig. 9 is increased until the pattern induced by the substrate patterning becomes completely stabilized. An example of such stable pattern is shown in Fig. 10.

V. CONCLUSIONS

We use the lubrication-type model of viscous flow coupled to the Debye-Hückel approximation for the electric field to investigate steady states, instabilities, and patterns in thin electrolyte films. A strongly nonlinear evolution equation for the film thickness is derived. Linear stability criteria are obtained by using the discretized version of the linearized equation for the interface shape, leading to an eigenvalue problem for the resulting matrix. Floquet theory is used in the regime when the domain size greatly exceeds the spatial scale of the substrate charge variation, L, making the direct numerical approach impractical and time consuming. Asymptotic expansions valid in the limit of small charge density variation amplitude δ were obtained to verify and interpret the numerical stability results.

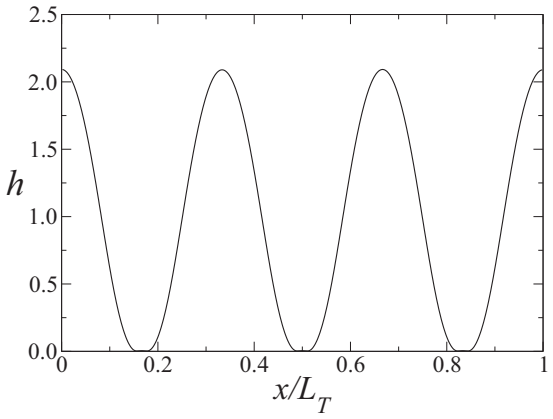

FIG. 10. Stable pattern which mimics the pattern of substrate charge density variation, observed at $\delta = 0.8$.

The main focus of our stability analysis is on the case of oppositely charged surfaces in the so-called nonresonant regime, i.e., the situation when evolution of the main instability mode is not affected by the resonant interaction with the substrate patterning. Several previous studies suggest that the correction to stability criteria should be very small, of the order δ^2. Surprisingly, we find this to be not the case in our model. For a range of values of L and κ, the effect is found to be stabilizing and increasing linearly with δ, based on both numerical and analytical results. To resolve the apparent contradiction, we invoke a simplified model which clearly shows the source of the discrepancy. The usual arguments regarding the nonresonant interaction implicitly assume that the correction to the threshold instability wave number is small. We find this to be not the case, explaining the observed behavior. We then varied the scaled length of the patterning in the same range of κ and observed that the effect changes from stabilizing to strongly destabilizing at some critical value of L. An analytical formula is derived for this critical value and is consistent with the numerical results. In practical terms, this implies that for a fixed amplitude of the charge density variation, the liquid film can become destabilized when the length scale of patterning is decreased.

Stronger than expected dependence of the stability threshold on the magnitude of the charge variation may seem surprising from the physical standpoint. Suppose the average dimensional substrate charge density q_a^* corresponds to the instability threshold. Intuitively, it may seem that the destabilizing effect of a region of higher $\tilde{q}^*$ should be compensated by the stabilizing effect of the region of lower value of the charge density, so that there is no net shift. However, this simplified argument ignores the different dependence of the stabilizing osmotic pressure, discussed above in Sec. III A, and destabilizing Maxwell stresses on the substrate charge density [37,38]. Our model is designed to consistently capture both of these physical effects.

Nonlinear evolution of unstable liquid films is investigated through a combination of weakly nonlinear analysis and numerical simulations, with the main focus on the types of patterns observed in the film and their dependence on the charge density pattern. While at smaller δ, the pattern wavelength is dictated by the intrinsic instability scale from the uniform substrate case, the larger δ shows increasingly dominant effect of the underlying charge pattern in the final shape of the free surface.

ACKNOWLEDGMENTS

The study was financially supported by the Russian Science Foundation (Project No. 16-19-10675). We are grateful to V. V. Shelukhin for valuable suggestions.

APPENDIX A

Assuming that the layer thickness is much smaller than the instability wavelength, the Stokes flow equations are reduced to the lubrication-type equations through the following procedure. The vertical and horizontal length scales are defined by d and $\mathrm{Ca}^{-1/3}d$, respectively, where $\mathrm{Ca} = \mu U/\sigma$ is the capillary number. The aforementioned scalings lead to the following nondimensional variables, respectively, for velocity components u^* and v^*, pressure p^*, and time t^*:

$$u = \frac{u^*}{U}, \quad v = \frac{v^*}{\mathrm{Ca}^{1/3}U}, \tag{A1}$$

$$p = \frac{\epsilon p^*}{q_a^{*2}}, \quad t = \frac{\mathrm{Ca}^{1/3}Ut^*}{3d}. \tag{A2}$$

After nondimensionalization, the governing equations have the form

$$p_x = u_{yy} + \psi\psi_x, \tag{A3}$$

$$p_y = \psi\psi_y, \tag{A4}$$

$$u_x + v_y = 0. \tag{A5}$$

The leading-order stress and kinematic conditions are

$$u_y = 0, \tag{A6}$$

$$p_0 - p = h_{xx} - \tfrac{1}{2}\hat{q}^2, \tag{A7}$$

$$\tfrac{1}{3}h_t = v - uh_x. \tag{A8}$$

Integrating Eq. (A3) with the condition (A6) and no slip at the substrate, the expression for fluid flow velocity is

$$u(y) = \tfrac{1}{2}(p_x - \psi\psi_x)(y^2 - 2hy). \tag{A9}$$

Using Eqs. (A5), (A7), and (A8), leads to the height evolution of the film given by (4).

APPENDIX B

The numerical solution of (17) involves spatial discretization of the domain $[-L_T, L_T]$ with N_T mesh points to reduce the problem to

$$\mathbf{z}_t = M\mathbf{z}, \tag{B1}$$

where $\mathbf{z}$ is the vector of the values of ζ at the mesh points and the entries of the matrix M are computed based on the standard centered finite-difference discretization of the spatial derivatives in (17). The neutral stability then corresponds to the condition when the maximum eigenvalue of the matrix M changes sign from negative to positive. We used MATLAB `fzero` subroutine to find this condition with the maximum

eigenvalue computed by `eig` subroutine; the initial guess for $\hat{\psi}$ is provided by the known analytical stability criterion for $\delta = 0$. Discretization uses $N_T = 2000$ grid points and simulations are conducted on SMU's High Performance Computing M2 cluster (306 nodes, 630 TFLOPS).

The numerical solution of the nonlinear equation (4) on the domain $[-L_T, L_T]$ was carried out using the method of lines with with finite-difference discretization of spatial derivatives and CVODE subroutine for time stepping.

APPENDIX C

Following the standard result of the weakly nonlinear analysis [23,33,34], stable patterns are possible near the instability threshold with the magnitude of the (complex) amplitude $\hat{A}$ which can be written in our notation as

$$|\hat{A}|^2 = -\frac{6\Phi_2\Phi_0}{[\varphi''(1)]^2 + 3\varphi'''(1)\varphi'(1)}, \tag{C1}$$

where Φ_2 measures the degree of departure from criticality. Note that the solution only exists when the right-hand side of the expression is positive. Formulas for quantities in the formula above are found by applying the weakly nonlinear analysis approach to the original nonlinear equation [Eq. (4)]. The resulting expressions are

$$\varphi'(1) = \frac{\kappa}{\cosh^3\kappa}(\hat{\psi}\sinh\kappa - 1)(\hat{\psi} + \sinh\kappa), \tag{C2}$$

$$\varphi''(1) = \frac{\kappa^2}{\cosh^4\kappa}\left\{[2 - \cos(2\kappa)](\hat{\psi}^2 - 1) + \frac{1}{2}\hat{\psi}\sinh\kappa[11 - \cosh(2\kappa)]\right\}, \tag{C3}$$

$$\varphi'''(1) = -4\kappa\tanh\kappa\varphi''(1) + \frac{\kappa^3}{\cosh^4\kappa}\left(2\sinh(2\kappa)(1 - \hat{\psi}^2) + \frac{\hat{\psi}}{2}\{\cosh\kappa[11 - \cosh(2\kappa)] - 2\sinh\kappa\sinh(2\kappa)\}\right). \tag{C4}$$

[1] A. Guenther and K. F. Jensen, Lab Chip **6**, 1487 (2006).
[2] V. S. Ajaev and G. M. Homsy, Annu. Rev. Fluid Mech. **38**, 277 (2006).
[3] O. A. Kabov, Thermophys. Aeromech. **7**, 513 (2000).
[4] O. A. Kabov, D. V. Zaitsev, V. V. Cheverda, and A. Bar-Cohen, Exp. Therm. Fluid Sci. **35**, 825 (2011).
[5] G. Celata, C. Colin, P. Colinet, P. D. Marco, T. Gambaryan-Roisman, O. Kabov, O. Kyriopoulos, P. Stephan, L. Tardist, and C. Tropea, Europhys. News **39**, 23 (2008).
[6] D. Zaitsev, M. L. Aviles, H. Auracher, and O. Kabov, Microgravity Sci. Technol. **19**, 71 (2007).
[7] O. Reynolds, Proc. R. Soc. London **40**, 191 (1886).
[8] A. Oron, S. H. Davis, and S. G. Bankoff, Rev. Mod. Phys. **69**, 931 (1997).
[9] R. Craster and O. Matar, Rev. Mod. Phys. **81**, 1131 (2009).
[10] E. Ruckenstein and R. K. Jain, J. Chem. Soc., Faraday Trans. **70**, 132 (1974).
[11] M. Williams and S. H. Davis, J. Colloid Interface Sci. **90**, 220 (1982).
[12] J. Burelbach, S. G. Bankoff, and S. H. Davis, J. Fluid Mech. **195**, 463 (1988).
[13] W. Zhang and J. Lister, Phys. Fluids **11**, 2454 (1999).
[14] H. Schulze, K. Stockelhuber, and A. Wagner, Colloids and Surfaces A. Physiochem. Eng. Aspects **192**, 61 (2001).
[15] A. Graciaa, G. Morel, P. Saulner, J. Lachaise, and R. Schechter, J. Colloid Interface Sci. **172**, 131 (1995).
[16] C. Li and P. Somasundaram, J. Colloid Interface Sci. **146**, 215 (1991).
[17] C. Ketelaar and V. S. Ajaev, Phys. Rev. E **89**, 032401 (2014).
[18] V. S. Ajaev, E. Y. Gatapova, and O. A. Kabov, Adv. Coll. Int. Sci. **228**, 92 (2016).
[19] P. Lenz, C. Bechinger, C. Schaefle, P. Leiderer, and R. Lipowsky, Langmuir **17**, 7814 (2001).
[20] K. Kargupta, R. Konnur, and A. Sharma, Langmuir **16**, 10243 (2000).
[21] K. Kargupta and A. Sharma, Phys. Rev. Lett. **86**, 4536 (2001).
[22] U. Thiele, L. Brusch, M. Bestehorn, and M. Bär, Euro. Phys. J. E **11**, 255 (2003).
[23] J. C. Kao, A. A. Golovin, and S. H. Davis, J. Colloid Interface Sci. **303**, 532 (2006).
[24] G. Krausch, Mater. Sci. Eng. Rep. **14**, 1 (1995).
[25] J. Ou, J. B. Perot, and J. P. Rothstein, Phys. Fluids **16**, 4635 (2004).
[26] V. S. Ajaev, E. Y. Gatapova, and O. A. Kabov, Phys. Rev. E **84**, 041606 (2011).
[27] L. Klausen, T. Fuhs, and M. Dong, Nat. Commun. **7**, 12447 (2016).
[28] V. V. Shelukhin and Y. Amirat, J. Appl. Mech. Tech. Phys. **49**, 655 (2008).
[29] I. Langmuir, Science **88**, 430 (1938).
[30] V. A. Parsegian and D. Gingell, Biophys. J. **12**, 1192 (1972).
[31] V. S. Ajaev, *Interfacial Fluid Mechanics: A Mathematical Modeling Approach* (Springer, Berlin, 2012).
[32] K. Kargupta, A. Sharma, and R. Khanna, Langmuir. **20**, 244 (2004).
[33] A. Oron and S. G. Bankoff, J. Colloid Interface Sci. **218**, 152 (1999).
[34] B. Y. Rubinstein and A. M. Leshansky, Phys. Rev. E **83**, 031603 (2011).
[35] U. Thiele, M. G. Velarde, and K. Neuffer, Phys. Rev. Lett. **87**, 016104 (2001).
[36] J. A. Diez and L. Kondic, Phys. Fluids **19**, 072107 (2007).
[37] G. Silbert, D. Ben-Yaakov, Y. Dror, S. Perkin, N. Kampf, and J. Klein, Phys. Rev. Lett. **109**, 168305 (2012).
[38] S. R. Maduar, V. Lobaskin, and O. I. Vinogradova, Faraday Discuss. **166**, 317 (2013).